Available online at www.sciencedirect.com
SCIENCE DIRECT®
Physica E 29 (2005) 87–99
PHYSICA E
www.elsevier.com/locate/physe

Intrinsically biased, resonant NEMS–MEMS oscillator and the second law of thermodynamics

D.P. Sheehan[a,*], J.H. Wright[b], A.R. Putnam[c], E.K. Perttu[a]

[a]Department Physics, University of San Diego, San Diego, CA 92110, USA
[b]Department Mathematics and Computer Science, University of San Diego, San Diego, CA 92110, USA
[c]Department Computer Engineering, University of Washington, Seattle, WA, USA

Available online 1 July 2005

Abstract

An experimentally testable NEMS–MEMS resonant cantilever oscillator is examined theoretically for compliance with the second law of thermodynamics. The device consists of a p–n semiconductor parallel-plate capacitor, with one plate fixed (p-doped) and the other (n-doped) mounted on a flexible double cantilever spring. The built-in potential across the n–p depletion region is expressed as an electric field between the capacitor plates, providing negative pressure capable of closing the plates. For matched electrical and mechanical time constants ($\tau_e \simeq \tau_m$), the device is predicted to execute steady-state electromechanical oscillation, powered solely by the p–n diodic electric field, thereby challenging the Kelvin–Planck formulation of the second law. Prospects for laboratory tests are discussed.

PACS: 77.65.−j

Keywords: Second law of thermodynamics; NEMS; MEMS; Oscillator; Cantilever

1. Introduction

The second law of thermodynamics—in its various formulations[1]—enjoys nearly universal support from the scientific community.[2] No experimental violation of it has been exposed during its 150-year history. Many believe it to be inviolable even in principle. Over the last decade, however, more than two dozen challenges to it have appeared in the refereed scientific literature [1–27]. While most are theoretical [3–14], several invite direct experimental test [15–27]. One broad

*Corresponding author. Tel.: +1 619 260 4095; fax: +1 619 260 6874.
E-mail address: dsheehan@sandiego.edu (D.P. Sheehan).

[1]There are many formulations of the second law, not all of which are equivalent. For example, 21 versions are cited by Čápek and Sheehan [1].

[2]Imprimaturs by eminent scientists like Einstein, Eddington and Brillouin are legion. See [1, Chapter 10].

1386-9477/$ - see front matter © 2005 Elsevier B.V. All rights reserved.
doi:10.1016/j.physe.2005.05.005

class of the latter, investigated at the University of San Diego (USD), exploits equilibrium macroscopic potential gradients, such as those found in the Debye sheaths at the edges of plasmas (electric field) [22,23], in the depletion regions of p–n junctions (electric field) [24–26], in the curved space time around planets (gravitational field) [14], and nearby chemically active surfaces in low-density gases (chemical potential field) [27].

The USD solid-state challenges are based on the cyclic electromechanical discharging and thermal recharging of the electrostatic energy derived from the depletion region of standard p–n junctions. The original solid-state system used this electrostatic energy to drive a dielectric piston cyclically in a vacuum gap, operating as a linear electrostatic motor (LEM) [24–26]. Like the LEM, the present challenge employs diodic electrostatic energy; however, it is superior in several respects. Its construction lies more squarely within the current art of micro- and nano-device fabrication, requiring less stringent machining than the LEM; it can be manufactured and tested today. It is more easily modeled analytically and numerically. Finally, it appears more amenable to experimental diagnosis.

The present device is a relative of well-studied NEMS and MEMS[3] cantilever oscillators. Cantilever oscillators have many proven and potential applications, including as accelerometers, motors, clocks, sensors (e.g., temperature, pressure, electronic charge, magnetic fields, environmental contaminants, microbes), beam steerers, choppers, and modulators, computing elements, and switches [30,31]. Cantilevers are usually driven by AC electrical signals whose frequencies are commensurate with their mechanical oscillation frequencies, but under suitable circumstances, DC signals can also effectively drive them. Owing to their utility and commercial applications, the art of NEMS–MEMS cantilevers is advanced.

DC-driven, resonant cantilevers have been investigated on a limited basis. In 1998, Bienstman et al. [32] introduced the concept of an "autonomous impact oscillator" in which DC-voltage is converted to AC-mechanical motion in relatively large silicon MEMS resonators. In this paper, we extend this concept down to micron and submicron scales—where surface effects become increasingly important—and we identify three general criteria for sustained resonant oscillation. A double cantilever prototype is parametrically analyzed within the specifications of a standard MEMS device fabrication process (Sandia National Laboratories' SUMMiT^{TM} V) using lightly doped polysilicon. It is found that resonant oscillation should be achievable at DC biases more than an order of magnitude smaller than those previously explored experimentally [32]. More significantly, it is shown that, with n–p doped silicon, self-sustained oscillation might be possible with zero external bias, relying instead on the intrinsic bias of the p–n diode depletion regions. This implies, however, the transformation of lattice heat solely into work, thereby compromising the Kelvin–Planck form of the second law.

2. Resonant electromechanical oscillation: hammer–anvil

In this section, we develop the theory of resonant oscillation for parallel-plate electromechanical oscillators. Consider the macroscopic electromechanical device pictured in Fig. 1a, consisting of a battery (V_0), resistor (R), and a variable capacitor in which the bottom plate (the *anvil*) is fixed, while the top plate (the hammer, mass m) is suspended from a conducting spring with spring constant k. This device will be called the *hammer–anvil*. It is a hybrid of well-known mechanical and LRC oscillators. The hammer is free to move with respect to the anvil and, when they contact, any accumulated charge on the plates is assumed to flow between them without resistance. The electrical capacitance of the device varies with the dynamic separation of the plates according to

$$C(y) = \frac{\varepsilon_0 A}{y_{\text{gap}} - y}, \tag{1}$$

where A is the area of the plates, y_{gap} is the equilibrium separation of the plates, and $y = y(t)$ is the instantaneous position of the hammer,[4] with the

[3]Nano-electro-mechanical systems/Micro-electro-mechanical systems [28,29].

[4]$y = 0$ is the static mechanical equilibrium position of the hammer.

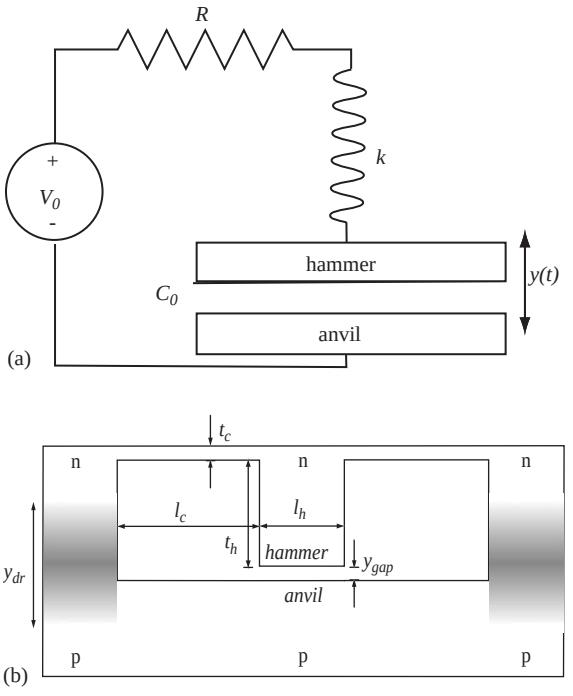

Fig. 1. Hammer–anvil electromechanical oscillator: (a) macroscopic device; (b) NEMS–MEMS cantilever device.

positive direction downward. We denote by $C_0 = \varepsilon_0 A/y_{\text{gap}}$ the capacitance when the spring is in its undeflected equilibrium state.

The electromechanics of the hammer is described by the coupled pair of equations:

$$F = F_{\text{diss}} + F_{\text{s}} + F_{\text{es}} = m\ddot{y} = -\frac{1}{Q}\dot{y} - ky - \frac{q^2}{2\varepsilon_0 A}, \tag{2}$$

where the instantaneous charge on the plates $q(t)$ satisfies:

$$\dot{q} = \left(V_0 - \frac{q(y_{\text{gap}} - y)}{\varepsilon_0 A}\right)\frac{1}{R}, \quad q < q_{\text{sat}}, \tag{3}$$

and $\dot{q} = 0$ for $q \geqslant q_{\text{sat}}$. Here the RHS of (2) gives of the dissipative, spring, and electrostatic forces, respectively. q_{sat} is the maximum (saturated) charge on the plates, set by geometry and composition of the plates.

Two independent time constants characterize this system: one electrical ($\tau_{\text{e}} \simeq RC_0$) and one mechanical ($\tau_{\text{m}} \simeq 2\pi\sqrt{m/k}$). This system can be electromechanically unstable: if the charged capacitor plates electrostatically draw together and electrically discharge, the attractive electric field collapses, the spring retracts the plates, the plates recharge on time scale τ_{e}, and the cycle can repeat. If the hammer's mechanical oscillation time constant is comparable to the circuit's electrical time constant, and if the quality factor (Q) is sufficiently large, then the system can sustain resonant electromechanical oscillation, converting the electrical energy of the battery into mechanical energy.

A macroscopic laboratory model based on Fig. 1a was built and tested (scale length ~50 cm); it validated the electromechanical principles of the hammer–anvil. The model consisted of a 60 cm long tungsten spring (spring constant $k = 0.8\,\text{N/m}$) attached to a mobile, circular capacitor plate (hammer, dia = 10 cm, $m = 4$ gm, metallic), suspended above a fixed metallic plate, in series with a variable resistor ($5 \times 10^4\,\Omega \leqslant R \leqslant 2 \times 10^7\,\Omega$) and power supply ($500\,\text{V} \leqslant V_0 \leqslant 2000\,\text{V}$). (A booster capacitor ($C_{\text{boost}} = 2\,\mu\text{F}$) was placed in parallel with the hammer–anvil capacitor to allow $\tau_{\text{m}} \sim \tau_{\text{e}}$.) As the resistance R was varied and the resonance condition was met ($\tau_{\text{e}} \simeq RC \simeq 2\pi\sqrt{m/k} \simeq \tau_{\text{m}}$), the hammer-capacitor fell into steady-state oscillation, while outside this regime, the oscillation either could not be started or, if it was jump-started, the oscillation quickly died out.

Fig. 2 depicts the operational status (OS) of the laboratory model at four bias voltages (500, 750, 1000, 1250 V). OS levels 1–4 on the ordinate correspond to: (1) no oscillation; (2) sub-harmonic or super-harmonic; (3) nearly harmonic; (4) harmonic oscillation. The abscissa gives the ratio of electrical to mechanical time constants ($\tau_{\text{e}}/\tau_{\text{m}}$), adjusted via the variable resistor R (Fig. 1a). These response curves are typical of forced resonant oscillators. As expected, Fig. 2 indicates harmonic response (OS-3,4) at $\tau_{\text{e}}/\tau_{\text{m}} \simeq 1$; and non-harmonic response elsewhere. The resonance peak shifts to higher $\tau_{\text{e}}/\tau_{\text{m}}$ values with increasing bias voltage. The OS-2 and OS-3 plateaus broaden with increasing bias voltage; this is consistent with the oscillator being driven harder and, thus, requiring less stringent ($\tau_{\text{e}}/\tau_{\text{m}}$) criterion to achieve gap

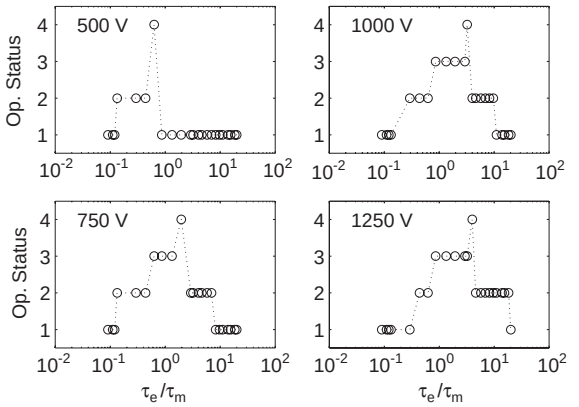

Fig. 2. Operational status (OS) of macroscopic laboratory model *hammer–anvil* versus ratio of electrical and mechanical time constants (τ_m/τ_e). Legend: (1) no oscillation; (2) sub-harmonic or super-harmonic oscillation; (3) nearly harmonic oscillation; (4) harmonic oscillation.

closure. Similar peak broadening is predicted for the MEMS or NEMS hammer–anvil.

3. Three operational criteria

In this section, three necessary and sufficient conditions for resonant electromechanical oscillation are developed for the hammer–anvil, scaled down to micro- and nanoscopic scales.

Consider the p–n device depicted in Fig. 1b, a microscopic version of the hammer–anvil, consisting of two p–n diodes (columns) on either side connected on top to a block of n-type material suspended by two flexible cantilever springs over the central p-type base. Comparing Figs. 1a and b, the top-center n-semiconductor mass in Fig. 1b acts as the hammer in Fig. 1a; likewise, the lower stationary p-semiconductor in Fig. 1b acts as the lower, fixed anvil. The spring is replaced by a double cantilever. For long, thin cantilevers ($t_c \ll l_c$) and for small vertical displacements ($y_{gap} \ll l_c$), a linear spring constant can be defined: $k = Yl_z/2[t_c/l_c]^3$, where l_c, l_z, and t_c are length, depth (into the page), and thickness, and Y is Young's modulus ($Y_{silicon} = 1.1 \times 10^{11}\,N/m^2$). The column depletion regions impose their built-in voltage across the central gap, similarly as for the externally biased hammer–anvil in Fig. 1a. This will be termed *intrinsic biasing* since no external voltage source is applied. This is in contradistinction to the traditional *extrinsic biasing* that drives everyday electronic devices.[5] Intrinsic biasing is examined in Section 4.

For the MEMS–NEMS hammer–anvil, force equation (2) still applies, but with the addition of a van der Waals force term, which becomes dominant with narrow gaps:

$$F_{vdW} = \frac{HA}{6\pi(y_{gap} - y)^3}. \tag{4}$$

Here H is the Hamaker constant ($H = 0.4 - 4 \times 10^{-19}$ J for most non-polar materials; for silicon $H_{Si} = 10^{-19}$ J).

The electric field in the gap (Fig. 1b) provides negative electrostatic pressure that drives and sustains the mechanical oscillations. For sustained oscillation—using either intrinsic or extrinsic biasing—three criteria must be met:

(I) The electrical and mechanical time constants must be comparable to achieve electromechanical resonance ($\tau_e \simeq \tau_m$).
(II) The hammer's mechanical energy gain per cycle ($\Delta\mathscr{E}_{es}$) must equal or exceed its mechanical dissipation ($\Delta\mathscr{E}_{diss}$), otherwise the oscillation will damp out; and
(III) The cantilever spring force F_s retracting the hammer after contact with the anvil must exceed the maximum van der Waals and electrostatic attractive forces ($F_s > F_{vdW} + F_{es}$), otherwise the hammer will stick to the anvil.

We address each criterion separately, then combine (II) and (III) into a more general form.

3.1. Criterion (I) (Electromechanical time constants)

The primary criterion for electromechanical resonance is that the hammer–anvil's characteristic electrical and mechanical time constants be

[5]The hammer–anvil can also be driven extrinsically with reverse biasing in Fig. 1b.

comparable; that is:

$$\tau_e \simeq \tau_m. \tag{5}$$

The electrical time constant τ_e for the hammer–anvil p–n junction (Fig. 1b) should be on the order of the inverse-slew rate of a comparably sized p–n diode. This is typically 10^{-6}–10^{-8} s for micron-size silicon diodes, corresponding to frequencies of $f_e \sim 1$–100 MHz. This puts a severe constraint on the oscillator's mechanical time constant and, consequently, requires that the oscillator be physically small and rugged so as to tolerate the large accelerations and stresses inherent in such high-frequency oscillation. For a harmonic oscillator with maximum physical displacement y_0 and angular frequency ω, the maximum acceleration scales as $\ddot{y}_0 \sim \omega^2 y_0$; thus for $\omega = 10^8$ rad/s, this implies $\ddot{y} \sim 10^{16} y_0$ m/s^2. Clearly, only small, rugged oscillators can survive the stresses of such accelerations.

The approximate resonant mechanical frequency of a double-cantilever (with negligible hammer mass) is given by

$$\frac{1}{\tau_m} = f_m \simeq B_n \sqrt{\frac{Y}{\rho}} \frac{t_c}{l_c^2}, \tag{6}$$

where B_n is a constant of order unity, and ρ is the mass density of the cantilever ($\rho_{Si} = 2.3 \times 10^3$ kg/m^3). For comparison, a silicon cantilever of dimensions $t_c = 10^{-6}$ m and $l_c = 10^{-5}$ m should have a resonant frequency of approximately $f_m \sim 10^8$ Hz.[6]

Since f_m can be made comparable to f_e, the first criterion appears capable of being met by NEMS or MEMS systems. Mechanical resonant frequencies for cantilevers in excess of 10^9 Hz have been achieved, however, the quality factors (Q) of these are significantly reduced, possibly due to dissipative surface states which can dominate the physics at short distance scales [33,34].[7]

[6]The mass of the hammer should lower this frequency.

[7]For initial experimental tests, f_e should be minimized so as to minimize f_m since this would admit physically larger devices, which are generally easier to fabricate and diagnose. Also, larger devices usually enjoy larger Q_s, which should reduce power requirements.

Good conductors (e.g., metals) and good insulators are not viable for construction of the hammer–anvil. One might suppose that two metals (M1 and M2) with differing work functions (Φ_1 and Φ_2) might replace the n- and p-doped semiconductors in Fig. 1b. After all, the difference in their work functions would be expressed as a potential difference ($\Delta V = (1/q)(\Phi_1 - \Phi_2)$) across the capacitor gap just as for the semiconductor case. Unfortunately, owing to their superior conductivity, the electrical time constants for metals τ_e are much shorter than any reasonable mechanical time constant τ_m; thus, electromechanical resonance condition ($\tau_e \simeq \tau_m$) cannot be met. At the opposite extreme of non-conductors (insulators), the electrical recharge time constant is too long, again foiling the resonance condition.

3.2. Criterion (II) (Work versus dissipation)

Criterion (II) requires that the energy gained through electrostatic work on the hammer per mechanical cycle ($\Delta\mathscr{E}_{es}$) exceed the mechanical dissipation per cycle ($\Delta\mathscr{E}_{diss}$). For typical MEMS–NEMS cantilevers, the relatively small sizes of the electrostatic and dissipative forces compared with the mechanical spring forces allow use of the harmonic approximation, which yields a closed-form integral solution to the coupled equations (2) and (3). Thus, we assume the hammer executes lightly damped ($Q \gg 1$) simple harmonic motion: $y(t) \simeq y_{gap} \cos(\omega_0 t)$, with $\omega_0 = \sqrt{k/m}$. Substituting this into (3) yields an uncoupled equation for the evolution of the electric charge on the capacitor plates:

$$\dot{q} + q \frac{(1 - \cos(\omega_0 t))}{RC_0} - \frac{V_0}{R} = 0, \tag{7}$$

whose solution for homogeneous initial conditions is

$$q(t) = \frac{V_0}{R} \exp[g(t)] \int_0^t \exp[-g(\tau')]\, d\tau', \tag{8}$$

where $\tau_m = 2\pi/\omega_0$, and $\kappa \equiv \tau_m/2\pi\tau_e$, and $g(t) = [\kappa \sin(2\pi t/\tau_m) - t/\tau_e]$. Here $\tau_e = RC_0$ need not be an RC time constant as for the macroscopic oscillator (Fig. 1a); rather it will likely be set by microscopic thermal processes, for instance,

charge carrier diffusion, generation and recombination rates.[8]

The Gaussian parallel-plate approximation $E = q/\varepsilon_0 A$ allows the electrostatic energy gain over one period of mechanical oscillation τ_m to be written as

$$\Delta\mathscr{E}_{es} = \oint F_{es}\,dy(t) = \int_0^{\tau_m} \frac{q^2(t)}{2\varepsilon_0}\left[-\frac{1}{\tau_m} y_{gap}\sin\left(\frac{t}{\tau_m}\right)\right] dt. \quad (9)$$

Meanwhile, for lightly damped oscillators ($Q \gg 1$), the dissipation can be expressed in terms of Q as

$$\Delta E_{diss} \simeq \frac{\pi k y_{gap}^2}{Q}. \quad (10)$$

Combining (9) and (10) yields the second criterion:

$$\frac{\Delta\mathscr{E}_{es}}{\Delta\mathscr{E}_{diss}} = \frac{-Q}{2\pi\varepsilon_0\tau_m k y_{gap}} \int_0^{\tau_m} q^2(t)\sin\left(\frac{t}{\tau_m}\right) dt. \quad (11)$$

Recall that resonant oscillation develops only for $\tau_e \simeq \tau_m$. Away from this condition (either $\tau_m \gg \tau_e$ or $\tau_m \ll \tau_e$), it can be shown (taking $\tau_e \to 0$ or $\tau_e \to \infty$ in Eq. (8)) that the electric field becomes essentially static, so there is no net energy gain per cycle ($\Delta\mathscr{E}_{es} \longrightarrow 0$), while ΔE_{diss} remains constant; thus the oscillation damps out. In the regime $\tau_e \simeq \tau_m$, however, the asymmetry critical to resonance is realized: more work is performed *on* the spring by the field during gap closure than is work performed *by* the spring *against* the field on gap opening. It is also required that the Q of the oscillator be sufficiently large that the energy gain per cycle exceeds the energy loss per cycle. For lightly damped oscillators, oscillation can be sustained with minimal energy input.

3.3. Criterion (III) (Non-stick hammer)

The third criterion arises from the disparity in magnitude and spatial variation of the strengths of the forces acting on the hammer during a cycle. For systems of interest, dissipative and electrostatic forces are subordinate to spring and van der Waals forces over the critical distances near where the hammer makes contact with the anvil.[9] For the hammer not to stick to the anvil, the spring force at $y = y_{gap}$ must exceed the sum of the electrostatic and van der Waals (vdW) forces at the latter's cut-off (saturation) distance, which is typically about $y_{c\text{-}o} \sim 1.6 \times 10^{-10}$ m, roughly an atomic radius. In this model, the dissipative and electrostatic forces act mechanically in a non-conservative fashion and can be of the same order of magnitude. The spring and vdW forces, on the other hand, are conservative and vary spatially with significantly different power laws and intrinsic strengths; that is, while the spring force varies as $F_s \sim y$, the vdW force varies as $F_{vdW} \sim [y_{gap} - y]^{-3}$. Because of the latter's stronger spatial dependence, it can exceed the spring force at small gap distances—leading to stiction—unless steps are taken to prevent it. By varying surface composition, the vdW force can be altered over roughly over an order of magnitude via the Hamaker constant, but it can be most directly and easily reduced by reducing the contact area between the surfaces.

Since the parameter space for viable hammer–anvil oscillators is broad, for the sake of clarity and because experimental prototypes will be pursued first in the MEMS regime, we devote the following discussion to parameters closely aligned with a well-known and specified MEMS production standard: the SUMMiT^{TM} process as developed and supported by Sandia National Laboratories.

In Fig. 3, the principal forces exerted on the hammer (excluding dissipation, which should be small) are plotted versus gap opening for three typical oscillators, as specified by cantilever length (10–90 μm). The electrostatic force is set by the extrinsic (or intrinsic) bias $V_0 = 0.6$ V, with an electric field saturating at a maximum strength of 2×10^7 V/m. (This follows the conservative assumption that the vacuum gap electric field strength will remain below the dielectric strength of silicon (3×10^7 V/m). This should render a conservative (under-) estimate of actual device performance.) The vdW force is presented for five

[8] The type, doping, and temperature of the semiconductor should have a strong influence on τ_e; for example, GaAs should have significantly shorter time constants than Si.

[9] In principle, the hammer need not contact the anvil if discharge occurs, for example, via tunneling. In this way, Criterion III can be ameliorated but not obviated.

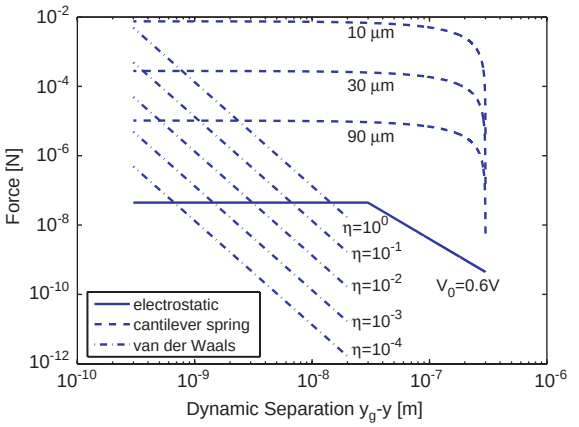

Fig. 3. Forces (N) on hammer versus dynamic separation (m) with anvil (SUMMiT^{TM} case). Spring force (dashed); van der Waals force (semidashed); electrostatic force (solid). Device parameters: $l_z = l_h = 5\,\mu m$, $t_c = 4.5\,\mu m$, $t_h = 6\,\mu m$, $l_c = 10, 30, 90\,\mu m$; $10^{-4} \leqslant \eta \leqslant 1$, $V_0 = 0.6\,V$.

values of surface contact fraction ($10^{-4} \leqslant \eta \leqslant 1$). As indicated by Fig. 3, for optimal designs of the *hammer–anvil*, η can be up to about $\eta \simeq 10^{-2}$, indicating 1% direct physical contact between hammer and anvil surfaces. Beyond this the hammer is expected to stick to the anvil.

The third criterion can be written $F_s > F_{vdW} + F_{es}$, or

$$ky_{gap} > \frac{H\eta A}{6\pi y_{c\text{-}o}^3} + \frac{\varepsilon_0 E_{max}^2 A}{2}. \tag{12}$$

Since $F_{es} \ll F_{vdW}$ in the contact region, the third criterion can be well approximated by

$$\frac{6\pi k y_{gap} y_{c\text{-}o}^3}{H\eta A} > 1. \tag{13}$$

If one sets the third criterion, (13), to equality and combines it with the second criterion, (11), one obtains a combined criterion:

$$\frac{Q}{4\pi\varepsilon_0^2 \tau_m k y_{gap}} \int_0^{\tau_m} q^2(t) \sin\left(\frac{t}{\tau_m}\right) dt > 1. \tag{14}$$

If one extracts the dimensional term q^2 from the integrand, assumes the integral resolves to order one, and re-expresses it slightly, an approximate, dimensionalized condition for steady-state operation can be written as

$$\frac{6\pi y_{c\text{-}o}^3 \varepsilon_0 E_{max}^2 Q}{\eta H} \simeq \frac{Q}{\eta} \frac{\text{Electrostatic pressure}}{\text{van der Waals pressure}} > 1. \tag{15}$$

This general condition connecting work, dissipation, and surface forces is the product of two simple ratios. The pressure ratio incorporates the pressure driving the oscillation (electrostatic) and the 'stiction pressure' (van der Waals), while the other ratio reflects the importance of minimum dissipation (Q) and minimum surface contact (η). Interestingly, the spring force, which figures prominently in both Criteria (II) and (III), drops out of this combined criterion entirely.

In summary, the three necessary and sufficient conditions for resonant electromechanical oscillation are embodied in Eqs. (5), (11) and (13); a more general, combined condition for the latter two is given by Eq. (15).

4. Intrinsic bias from a p–n junction

The heart of the hammer–anvil's paradoxical behavior rests in the built-in potential of the p–n depletion region. All present-day electronic devices require an *extrinsic* source of free energy to operate. This can be supplied in various forms, including electromagnetic radiation (IR, IV, visible, X-ray, etc.), chemical energy, or electronic energy in the form of current and voltage from an *external* power source. Standard cantilever oscillators are also powered via extrinsic bias, but the p–n diode hammer–anvil (Fig. 1b)—even in the absence of external bias—contains an *intrinsic* built-in bias V_{bi} across the vacuum gap (typically $V_{bi} \leqslant 1\,V$), which in principle can be cyclically exploited to perform work. As indicated in Fig. 1b, this *intrinsic bias* is due to the n–p junction's depletion regions in the columns supporting the cantilevers.

The depletion region of a standard p–n diode represents a minimum free energy state in which bulk electrostatic and diffusive forces are balanced. Typical depletion regions are narrow, ranging from 10 μm for lightly doped semiconductors to

0.01 μm for heavily doped ones. The potential drop across a depletion region, the built-in potential V_{bi} is given approximately by [35]:

$$V_{bi} = \frac{kT}{q} \ln\left(\frac{N_A N_D}{n_i^2}\right). \quad (16)$$

Here kT is thermal energy; q is electronic charge; n_i is intrinsic carrier concentration (for silicon ($n_i \simeq 1.2 \times 10^{16}\,\mathrm{m}^{-3}$ at 300 K); and $N_{A,D}$ are acceptor and donor concentrations. For dopant concentrations $N_A = N_D = 10^{21}\,\mathrm{m}^{-3}$, one has $V_{bi} \simeq 0.6\,\mathrm{V}$.

The built-in potential of the depletion region must be expressed across the hammer–anvil gap; this can be argued either via energy conservation (Kirchhoff's loop law) or via Faraday's law. Applying Kirchhoff's law, consider a closed loop that threads the bulk of the hammer–anvil through the gap and one column's depletion region (Fig. 1b). Conservation of energy demands that a test charge conveyed around this closed path must undergo zero net potential drop; therefore, to balance V_{bi} in the depletion region, there must be a counter-potential somewhere else in the loop. Since, at equilibrium, away from the depletion region there cannot be a potential drop (electric field) in the bulk semiconductor—otherwise there would be a non-equilibrium current flow, contradicting the assumption of equilibrium—the potential drop must occur outside the semiconductor; thus, it must be expressed across the vacuum gap. Alternatively, one can invoke Faraday's law for electrostatics ($\oint \mathbf{E}\,\mathrm{d}\mathbf{l} = 0$) to reach the same conclusion. Numerical simulations, using state-of-the-art semiconductor device simulators (e.g., Silvaco International—Atlas), verify this electric field.

Although V_{bi} is small, the gap width y_{gap} can also be made small such that the gap electric field—and therefore the electrostatic pressure—can be sizable. For example, for $V_{bi} = 0.6\,\mathrm{V}$ and gap width $y_{gap} = 3 \times 10^{-8}\,\mathrm{m}$, the gap field is $E \simeq V_{bi}/y_{gap} = 2 \times 10^7\,\mathrm{V/m}$ and pressure $P \simeq 10^3\,\mathrm{Pa}$. It is found both analytically and in numerical simulations that the gap electric field can store significant capacitive electrostatic energy ($\rho \equiv (\varepsilon_0/2E^2)$) which, in principle, can exceed that in a comparably sized depletion region. The open-gap hammer–anvil configuration in Fig. 1b is a high-energy equilibrium state. If the gap is closed a new equilibrium state is created, characterized by a new depletion region. The energy difference between these two equilibria can, in principle, drive the hammer–anvil. A more detailed account of the gap electric field is presented elsewhere [1,24].

5. Numerical simulations

Numerical simulations using MatLab and commercial semiconductor device simulators verify the principal results of the above one-dimensional model for both the extrinsically and intrinsically biased hammer–anvil. Two-dimensional numerical simulations of the system's electrical behavior, performed using Silvaco International's Semiconductor Device Simulation Software [Atlas (S-Pisces, Giga)], verify the equilibrium aspects of the intrinsic electric field in the gap. Output from the simulations was the steady-state, simultaneous solutions to the Poisson, continuity, and force equations, using the Shockley–Read–Hall recombination model. These show that the magnitude of the open-gap intrinsic electric field can exceed that of the local depletion region by almost an order of magnitude, topping out in excess of $10^7\,\mathrm{V/m}$. Although the gap volume is significantly less than the depletion region volume ($y_{gap} \ll y_{dr}$), since electrostatic energy density is proportional to E^2, the electrostatic potential energy of the open gap can significantly exceed that of the depletion region. Numerical simulations also verify that the electric field and electrostatic energy in the gap is lost upon gap closure as a new depletion region forms.

The electrostatic pressure P_{es} for the open-gap hammer–anvil with intrinsic biasing (e.g., $V_{bi} \simeq 0.6\,\mathrm{V}$) will be $P_{es} \simeq 10^3\,\mathrm{Pa}$. Although the absolute electrostatic force exerted on the hammer is small, under Criteria (I–III) it can be sufficient to resonantly drive and maintain a high-Q oscillation. NEMS–MEMS cantilevers have documented Q_s as high as $Q \sim 10^5$ in vacuum [33]. This implies that a small energy gain per cycle (e.g., $\sim 10^{-5}$ total mechanical energy) should be sufficient to sustain oscillation. In order to explore these claims, two

test cases are examined. The first involves a MEMS devices modeled within the specifications of Sandia National Laboratories SUMMiT^{TM} process, a standardized MEMS fabrication process for undoped polysilicon. This is chosen because the extrinsic hammer–anvil concept is currently being put to experimental test with SUMMiT^{TM} devices. Unfortunately, the size and specifications of this process preclude intrinsic biasing; still, these extrinsically biased devices should serve as touchstones and testbeds for future intrinsically biased devices. The second test case extends the hammer–anvil to smaller dimensions and to true intrinsic biasing where the second law challenge emerges.

In Fig. 4 is plotted a range of viability for hammer–anvil devices constructed with physical dimensions achievable with SUMMiT^{TM} V, and identical with the $l_c = 30\,\mu m$ case from Fig. 3. Fig. 4 presents the minimum bias voltage required for sustained mechanical oscillation consistent with Criteria (I–III), incorporating realistic physical parameters for silicon-based devices. Voltages are plotted as a function of quality factor Q and the ratio of electrical to mechanical time constants (τ_m/τ_e). Equipotentials (0.6–90 V) are overlayed

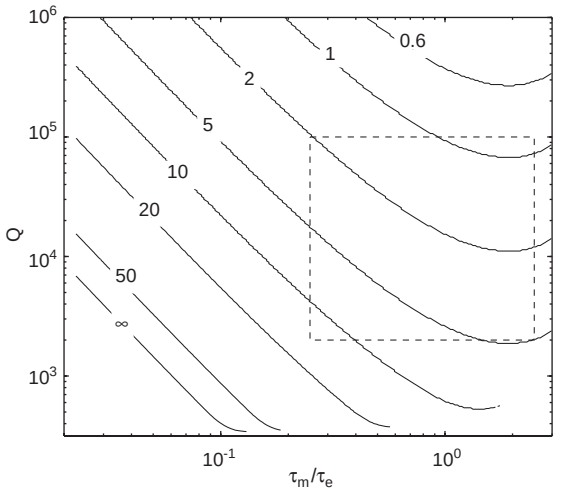

Fig. 4. *Extrinsically biased hammer–anvil*. External bias voltage required for sustained oscillation for SUMMiT^{TM} V device (Fig. 1b), plotted versus Q and τ_m/τ_e. In sweet spot ($0.25 \leqslant \tau_m\tau_e \leqslant 2.5$; $2\times10^3 \leqslant Q \leqslant 10^5$, interior of dashed box), low DC-voltage ($1\,V \leqslant V \leqslant 10\,V$) drives oscillation.

for comparison. Simulations are bounded above by the condition: $Q < 10^6$. The ∞-contour divides viable from unviable regions of parameter space; in the latter dissipation exceeds the maximum theoretical reactive energy available and oscillation cannot be sustained.

As indicated by Fig. 4, the hammer–anvil performs most efficiently (i.e., at the lowest DC-voltage) at the resonance condition ($\tau_m/\tau_e \sim 1$) and at large Q values. Away from these optimal conditions, either large driving voltages are required (e.g., $V_0 = 50\,V$ for $\tau_m/\tau_e \sim 10^{-1}$, $Q \sim 10^3$) or else the device fails entirely. In the sweet spot of Fig. 4 ($0.25 \leqslant \tau_m/\tau_e \leqslant 2.5$; $2\times10^3 \leqslant Q \leqslant 10^5$, interior of dashed box), the device can be driven at relatively low voltages ($1\,V \leqslant V_0 \leqslant 10\,V$) and should have a resonant electromechanical frequency of about $f \sim 1$ MHz. Note the hammer–anvil should be viable at $V_0 = V_{bi} \simeq 0.6\,V$, which is achievable even under intrinsic bias, but this requires a relatively high Q, which is probably not achievable with SUMMiT^{TM} V. This 0.6 V hammer–anvil is almost macroscopic in size (maximum dimension $\sim$0.1 mm).

The second test case, the *intrinsically biased hammer–anvil*, follows closely on the heels of case 1, but is free of the narrow constraints of SUMMiT^{TM}, thereby allowing n–p doping and a full choice of the critical dimensions that determine device performance, namely, N_A, N_D, y_{gap}, η, l_c, and t_c. In Figs. 5–7 are presented predicted performance summaries for the intrinsically biased hammer–anvil for three representative sets of fabrication parameters. For all figures, the carrier concentration levels (in crystalline silicon) are $N_A = N_D = 10^{21}\,m^3$, thereby fixing the built-in and gap biases at $V_{gap} = V_{bi} = 0.6\,V$, as given by Eq. (16). (Individual fabrication parameters are given in each figure caption.) Figs. 5–7(a) are logarithmic plots of the ratio τ_m/τ_e versus cantilever length, presenting contours of constant Q required for self-sustained oscillation under intrinsic bias alone. Figs. 5–7(b) plot mechanical frequency versus cantilever length.[10]

[10]Finite element modeling using Ansys indicates that with these choices of cantilever dimensions the fundamental vibrational modes of the cantilever are well separated in frequency from higher order flexing and torsional modes.

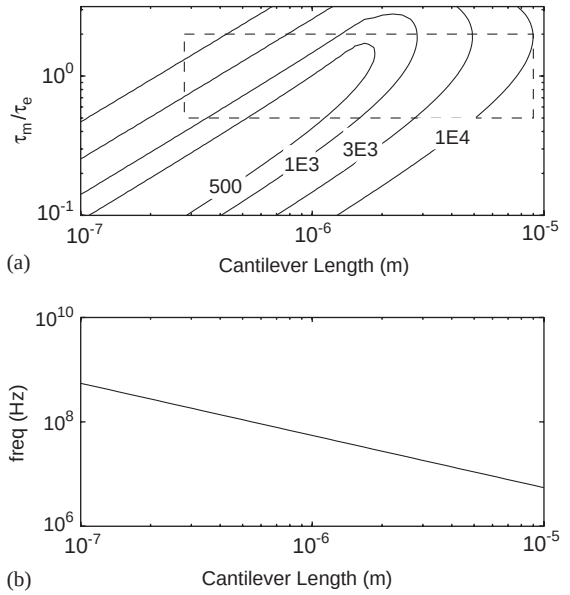

Fig. 5. Performance parameters for MEMS–NEMS cantilever hammer–anvil with $\eta = 0.0005$; $y_{gap} = 0.01l_c$; $t_c = 0.05l_c$; and $t_h = 2t_c = 0.10l_c$. NOTE: The following is common to Figs. 5–7: (a) Contours of constant Q plotted for τ_m/τ_e versus cantilever length; sweet spot located within boundaries of dashed lines. (b) Mechanical oscillation frequency versus cantilever length. Device dimensions (see Fig. 1b) set as ratios of cantilever length l_c: $l_h = 0.25l_c$; and $l_z = l_c$.

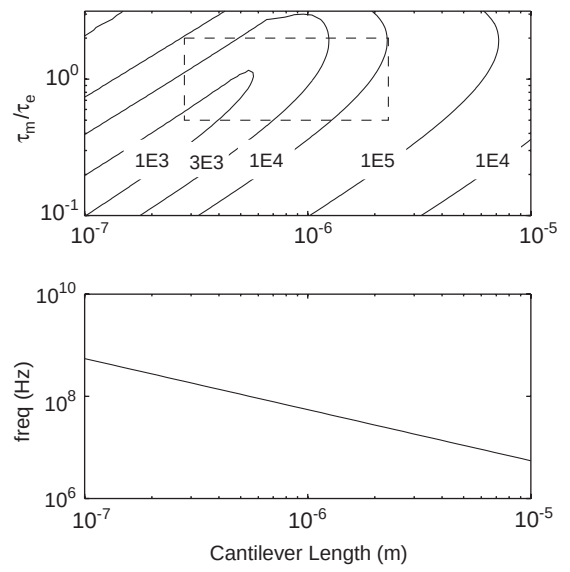

Fig. 6. Performance parameters for MEMS–NEMS cantilever hammer–anvil with $\eta = 0.001$; $y_{gap} = 0.025l_c$; $t_c = 0.05l_c$; and $t_h = 2t_c = 0.10l_c$. See NOTE in Fig. 5 caption for details.

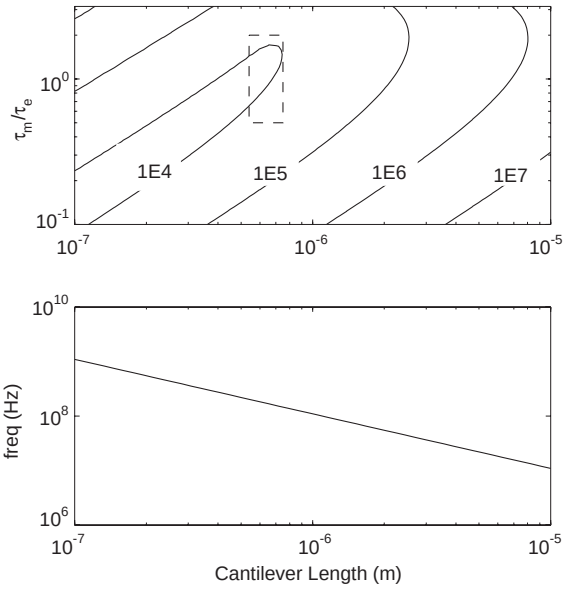

Fig. 7. Performance parameters for MEMS–NEMS cantilever hammer–anvil with $\eta = 0.01$; $y_{gap} = 0.025l_c$; $t_c = 0.10l_c$; and $t_h = 2t_c = 0.20l_c$. See NOTE in Fig. 5 caption for details.

All three criteria (Section 3) are evident in these plots and are useful in identifying the sweet spots of device operation. The starting point for this will be the surface contact fraction, η. For Figs. 5–7, η follows the progression $\eta = 5 \times 10^{-4}$, 10^{-3}, and 10^{-2}. Large η implies strong surface stiction (F_{vdW}) and thus requires a stiff cantilever (large t_c or short l_c) to assure retraction, which in turn implies a large Q. Clearly, $\eta \simeq 1$ would be ideal since this would essentially obviate the restrictions of Criterion III, but practically speaking it implies unrealistically large Q—this based on upper values of $Q \leqslant 10^5$ attained in laboratory studies. As a conservative estimate, we take $Q \leqslant 10^4$ for this hammer–anvil. This Q appears to restrict the surface contact fraction to values $\eta \leqslant 10^{-2}$ for realistic surfaces.[11] Criterion II is implicitly met in the generation of the Q contours.

Electromechanical resonance (Criterion I) is most favorable near $\log(\tau_m/\tau_e) = 0$ in Figs. 5–7(a). For this discussion, we take the range of

[11] $\eta = 10^{-2}$ translates to surface contact between the hammer and anvil of on the order of 10^5 atoms/μm^2.

viability to be within a factor of 2 of this; i.e., $0.5 \leqslant \tau_m/\tau_e \leqslant 2$. Numerical simulations of cantiliver dynamics verify robust oscillations in this regime. These limits are demarked by the horizontal dashed lines in Figs. 5–7(a). The characteristic electrical time constants for diodes is conservatively 10 ns $\leqslant \tau_e \leqslant 100$ ns. Under the condition $0.5\tau_e < \tau_m < 2\tau_e$, this bounds the mechanical frequency in Figs. 5–7(b) at $5 \times 10^6 < f_m < 2 \times 10^8$ Hz.

The operational sweet spot can be roughly circumscribed through consideration of f_m, Q and τ_m/τ_e. The sweet spots appear in Figs. 5–7(a) as rectangles bounded by vertical and horizontal dashed lines. As an example of their construction, consider Fig. 6. In Fig. 6b, the limits on f_m delimit the cantilever length to $3 \times 10^{-7} \leqslant l_c \leqslant 10^{-5}$ m. These l_c-limits can be carried up to Fig. 6a. The lower limit ($l_c \simeq 3 \times 10^{-7}$ m) holds, but the earlier constraint, $Q \leqslant 10^4$, lowers the upper l_c-limit to $l_c \leqslant 2 \times 10^{-6}$ m. These establish the vertical lines of the sweet spot. Meanwhile, the condition $0.5 \leqslant \tau_m/\tau_e \leqslant 2$ sets the horizontal bounding lines. Thus, the sweet spot in Fig. 6a appears as the interior of the rectangle with bounds $0.5 \leqslant \tau_m/\tau_e \leqslant 2$ and $3 \times 10^{-7} \leqslant l_c \leqslant 2 \times 10^{-6}$ m.

In general, the size of the sweet spot is inversely proportional to η, as evidenced in Figs. 5–7. For example, the sweet spot in Fig. 5b ($\eta = 0.0005$) spans a factor of 70 in l_c, while in Fig. 7b ($\eta = 0.01$), it spans only a factor of 2. If small contact fractions ($\eta \leqslant 10^{-2}$) are sufficient for operation, then there appear to be significant parameter ranges over which intrinsically biased hammer–anvils might be expected to thrive.

In theory, the device output power P_{dev} should scale as: $P_{dev} \sim f_m E_s/Q = f_m k y_{gap}^2/2Q$, where $E_s = k y_{gap}^2/2$ is the maximum elastic energy in the cantilever. For comparison, we take as a *standard device* one in the sweet spot of Fig. 6a, with $Q = 3 \times 10^3$ and $l_c \simeq 10^{-6}$ m. The instantaneous power for a single *standard device* should be small, roughly $P_{dev} \simeq 4 \times 10^{-11}$ W; however, its instantaneous power density can be appreciable; for the *standard device* should be on the order of $\mathscr{P}_{dev} \sim 10^7\ \mathrm{W m^{-3}}$. To put this in perspective, 100 $\mathrm{m^3}$ of these devices (amounting to about 3×10^{19} in number) could, in principle, convert thermal energy into work with instantaneous power output on par with the output of a modern-day nuclear power plant. This, of course, is only *instantaneous* power density since, were the device to convert thermal energy into work at this rate without compensatory heat influx from the surroundings, the device would cool at an unsustainably fast rate of about 1 K/s. When T fell below the freeze-out temperature for charge carriers—for silicon, $T_{freeze} \leqslant 100$ K—energy extraction would cease.

In summary, analysis indicates that high-Q MEMS–NEMS cantilevers, in principle, can achieve self-sustained resonant oscillation, utilizing intrinsic bias from a p–n depletion region. Simulations suggest a broad, physically realistic, and experimentally accessible parameter space in which the hammer–anvil might be sought.

6. Second law challenge

In principle, the steady-state operation of the intrinsically biased hammer–anvil represents a *perpetuum mobile* against which the second law reserves its strongest injunctions.[12] It is not evident how this paradox can be favorably resolved. The most obvious resolution is to posit that the hammer–anvil mechanical and electrical oscillations—which are individually well-documented—somehow critically interfere with one another, forbidding resonant oscillation between the two. This seems unlikely. The electrical characteristics of the device are physically independent of its mechanical characteristics. The depletion region and gap electric field depend on charge carrier number $N_{A,D}$, temperature T, and gap widths y_{gap}, while the device's mechanical characteristics (vibrational frequency and amplitude) depend on Young's modulus Y, mass density ρ, beam

[12]We emphasize that the second law is an experimental observation about the world, therefore no challenge to it can be considered a violation until it is supported fully by experiment. Conversely, however, a challenge cannot be dismissed out of hand simply by appealing to the second law itself; rather, it must fall to some other physical law, or to experiment.

thickness t_c and length l_c. Since these are physically independent of each other, it is not evident how either type of oscillation could cripple the other; rather, since they can be independently set and maintained, they should be able to support one another resonantly.

As a second line of defense, one might suppose that nature somehow conspires to make the damping or surface sticking criteria (II,III) impossible to meet for any physically realistic system, but as is shown above, estimates based on realistic parameters indicate that they can be met. In all, Criteria I–III—the necessary and sufficient conditions for resonant oscillation—offer no apparent escapes from the paradox.

For objects in this size range, the effect of statistical fluctuations should not be overlooked, especially since they have been the foil of many past challenges. Since the hammer–anvil exploits both elastic mechanical energy and capacitive electrostatic energy, it is sufficient to consider fluctuations of the former. If one equates the cantilever spring energy $\frac{1}{2}ky^2$ to the thermal energy $\frac{1}{2}k_BT$, then for the *standard device* at room temperature the thermally driven fluctuations in gap width should be on the order of $\Delta y \sim 10^{-11}$ m, or $\Delta y/y_{gap} \simeq 2 \times 10^{-4}$; thus, fluctuations should not appreciably affect the system's operation. A similar conclusion can be reached from a more detailed spectral analysis in the spirit of the Nyquist and Wiener–Khintchine theorems with respect to the rms charge fluctuation and the capacitive energy.

7. Experimental prospects

Prospects are good for laboratory construction and testing of the hammer–anvil in the near future. Present-day micro- and nano-manufacturing techniques are adequate to construct the device, especially since cantilevers are among the most avidly studied and fabricated MEMS–NEMS structures. The art of surface finishing, which is crucial to reducing friction and stiction, is the most problematic. State-of-the-art molecular beam epitaxy can reliably deposit layers to monolayer precision, but control of surface states is still difficult. Self-assembly of the requisite surfaces is plausible. Large scale biotic systems (e.g., DNA, microtubules) are well-known to self-assemble with atomic precision, as are abiotic ones (e.g., carbon nanotubes [36]). Control of impurity doping ($N_{A,D}$) presents no major problems. Diagnosis of oscillation amplitude and frequency are relatively straightforward.

The most sensitive device dimensions and tolerances occur in the *hammer–anvil* gap. Optimal gap width will probably be less than 0.1 μm. The contacting surfaces must be highly parallel and their morphology must be tightly controlled so as to meet the condition of low-contact fraction ($\eta \ll 1$). Contact wear will probably place limits on the total number of oscillations the device can execute [37]; however, this is not directly germane to the second law challenge.

The hammer–anvil envisioned here will almost certainly require a kick start since the maximum achievable electrostatic pressure, although sufficient to sustain oscillation, appears insufficient to initiate it. The kick start could be delivered in a number ways, including: (a) a large, transient DC voltage spike across the gap; (b) a small, short-lived, resonant, AC tickler voltage; or (c) piezoelectric AC mechanical drive of the entire device. Device operation might be monitored either by laser interferometry of the hammer's motion, or by coupling its vibrational energy to piezoelectric sensors. The latter would be propitious since, in principle, a piezo could be used both to jump start the oscillation and to detect it.

Tests of the hammer–anvil concept are currently being pursued. Extrinsically biased devices have been designed in SUMMiT^{TM} V and will soon be fabricated and laboratory tested. Intrinsically biased devices are in the design phase and are currently awaiting funding.

Acknowledgements

This work was supported by a USD Faculty Research grant and a Cottrell College grant from the Research Corporation. A. Ellefson is thanked for her assistance in numerical simulations.

References

[1] V. Čápek, D.P. Sheehan, Challenges to the Second Law of Thermodynamics—Theory and Experiment, Fundamental Theories of Physics, vol. 146, Springer, Dordrecht, Netherlands, 2005.

[2] D.P. Sheehan (Ed.), First International Conference on Quantum Limits to the Second Law, AIP Conference Proceedings, vol. 643, AIP Press, Melville, NY, 2002.

[3] L.G.M. Gordon, Found. Phys. 11 (1981) 103;
L.G.M. Gordon, Found. Phys. 13 (1983) 989;
L.G.M. Gordon, J. Coll. Interf. Sci. 162 (1994) 512;
L.G.M. Gordon, Entropy 6 (2004) 38,87,96.

[4] J. Denur, Am. J. Phys. 49 (1981) 352;
J. Denur, Phys. Rev. A 40 (1989) 5390;
J. Denur, Entropy 6 (2004) 76.

[5] V. Čápek, J. Phys. A 30 (1997) 5245;
V. Čápek, Czech. J. Phys. 48 (1998) 993;
V. Čápek, Czech. J. Phys. 47 (1997) 845;
V. Čápek, Czech. J. Phys. 48 (1998) 879;
V. Čápek, Mol. Cryst. Liq. Cryst. 335 (2001) 24.

[6] V. Čápek, J. Bok, J. Phys. A 31 (1998) 8745;
V. Čápek, Physica A 290 (2001) 379.

[7] V. Čápek, T. Mančal, Europhys. Lett. 48 (1999) 365;
V. Čápek, T. Mančal, J. Phys. A 35 (2002) 2111.

[8] V. Čápek, D.P. Sheehan, Physica A 304 (2002) 461.

[9] J. Bok, V. Čápek, Entropy 6 (2004) 57.

[10] A.E. Allahverdyan, Th.M. Nieuwenhuizen, Phys. Rev. Lett. 85 (2000) 1799;
A.E. Allahverdyan, Th.M. Nieuwenhuizen, Phys. Rev. E 64 (2001) 056117;
A.E. Allahverdyan, Th.M. Nieuwenhuizen, Phys. Rev. B 66 (2003) 115309;
A.E. Allahverdyan, Th.M. Nieuwenhuizen, J. Phys. A 36 (2004) 875.

[11] Th.M. Nieuwenhuizen, A.E. Allahverdyan, Phys. Rev. E 66 (2002) 036102.

[12] B. Crosignani, P. Di Porto, Am. J. Phys. 64 (1996) 610;
B. Crosignani, P. Di Porto, Europhys. Lett. 53 (2001) 290.

[13] B. Crosignani, P. Di Porto, C. Conti, in: Quantum Limits to the Second Law, p. 267; arXiv:physics/0305072v2 (2003);
B. Crosignani, P. Di Porto, C. Conti, Entropy 6 (2004) 50.

[14] D.P. Sheehan, J. Glick, J.D. Means, Found. Phys. 30 (2000) 1227;
D.P. Sheehan, J. Glick, T. Duncan, J.A. Langton, M.J. Gagliardi, R. Tobe, Found. Phys. 32 (2002) 441.

[15] A. Trupp, in: Quantum Limits to the Second Law, p. 201, 231.

[16] P. Keefe, J. Appl. Opt. 50 (2003) 2443;
P. Keefe, Entropy 6 (2004) 116.

[17] J. Berger, Phys. Rev. B 70 (2004) 024524.

[18] S.V. Dubonos, V.I. Kuznetsov, I.N. Zhilyaev, A.V. Nikulov, A.A. Firsov, JETP Lett. 77 (2003) 371.

[19] A.V. Nikulov, Phys. Rev. B 64 (2001) 012505.

[20] A.V. Nikulov, I.N. Zhilyaev, J. Low Temp. Phys. 112 (1998) 227.

[21] C. Pombo, A.E. Allahverdyan, Th.M. Nieuwenhuizen, in: Quantum Limits to the Second Law, p. 254.

[22] D.P. Sheehan, Phys. Plasmas 2 (1995) 1893;
D.P. Sheehan, Phys. Plasmas 3 (1996) 104.

[23] D.P. Sheehan, J.D. Means, Phys. Plasmas 5 (1998) 2469.

[24] D.P. Sheehan, J.H. Wright, A.R. Putnam, Found. Phys. 32 (2002) 1557.

[25] J.H. Wright, in: First International Conference on Quantum Limits to the Second Law, p. 308;
A.R. Putnam, First International Conference on Quantum Limits to the Second Law, 2002, p. 314.

[26] J.H. Wright, D.P. Sheehan, A.R. Putnam, J. Nanosci. Nanotech. 3 (2003) 329.

[27] D.P. Sheehan, Phys. Rev. E 57 (1998) 6660;
D.P. Sheehan, Physica A 280 (2001) 185.

[28] G. Timp (Ed.), Nanotechnology, Springer, New York, 1999.

[29] W. Trimmer (Ed.), Micromechanics and MEMS: Classic and Seminal Papers to 1990, IEEE Press, New York, 1997.

[30] J.A. Pelesko, D.H. Bernstein, Modeling MEMS and NEMS, Chapman & Hall/CRC, Boca Raton, 2003.

[31] M.L. Roukes, in: Technical Digest of the 2000 Solid-State Sensor and Actuator Workshop, Hilton Head Isl, SC, 2000.

[32] J. Bienstman, J. Vandewalle, R. Puers, Sensors and Actuators A 66 (1998) 40.

[33] P. Mohanty, D.A. Harrington, K.L. Ekinci, Y.T. Yang, M.J. Murphy, M.L. Roukes, Phys. Rev. B 66 (2002) 085416.

[34] R. Lifshitz, M.L. Roukes, Phys. Rev. B 61 (2000) 5600.

[35] G.W. Neudeck, The pn Junction Diode, in: R.F. Pierret, G.W. Neudeck (Eds.), Modular Series on Solid State Devices, vol. II, second ed., Addison-Wesley, Reading, 1989.

[36] M.S. Dresselhaus, G. Dresselhaus, P. Avouris (Eds.), Carbon Nanotubes—Synthesis, Structure, Properties and Applications, Springer, Berlin, 2001.

[37] K. Komvopoulos, Wear 200 (1996) 305.